Manufacturing Letters 31 (2022) 110–115

Contents lists available at ScienceDirect

Manufacturing Letters

journal homepage: www.elsevier.com/locate/mfglet

Two-photon polymerization of anisotropic composites using acoustic streaming

Ketki M. Lichade [a], Shan Hu [b], Yayue Pan [c,*]

[a] Department of Mechanical and Industrial Engineering, University of Illinois at Chicago, Chicago, IL 60607, United States
[b] Department of Mechanical Engineering, Iowa State University, Ames, IA 50011, United States
[c] Department of Mechanical and Industrial Engineering, University of Illinois at Chicago, Chicago, IL 60607, United States

ARTICLE INFO

Article history:
Received 20 April 2021
Received in revised form 30 July 2021
Accepted 2 September 2021
Available online 8 September 2021

Keywords:
Two-photon polymerization
Anisotropic composite
Acoustic streaming
Particle patterning

ABSTRACT

In this work, an acoustic streaming-assisted Two-Photon Polymerization process (TPP) was developed for manufacturing anisotropic particle-polymer composites. Acoustic field (AF)-assisted constant microcirculation of nanoparticles within a droplet, also known as acoustic streaming (AS), results in nanoparticle trapping within TPP printed grooved surfaces. The effect of the acoustic voltage on the flow velocity and particle trapping efficiency is modeled and characterized. The identified optimum input voltage was used to generate the proper acoustic streaming to trap particles within polymer grooves during TPP process to produce a three-dimensional (3D) anisotropic particle-polymer composite in a layer-by-layer fashion. Experimental results validated the feasibility of the proposed manufacturing approach.

1. Introduction:

Anisotropic composite structures have attracted much attention because of their remarkable enhancement in mechanical, electrical, and thermal properties [1–3]. The rapidly increasing demand for anisotropic composite micro/nanostructures in various applications, including bio-sensors [4], microelectronics, and energy storage [5,6], has necessitated the need to develop manufacturing techniques with precise spatial control of composite material. For instance, Kaneko et al. [7] studied the effect of anisotropic composite surface on the adhesion and growth of HeLa cells. First, the octadecyltrichlorosilane (OTS) substrate was prepatterned into linear arrays (50 μm wide) via stamping. Finally, silica particles (1 μm) were self-assembled between line patterns using Dip-coating. It was observed that the substrate acted as a template to automatically patterns cells into straight lines. Unlike the conventional indirect methods, Two-Photon Polymerization (TPP) is one of the most advanced technology for the direct fabrication of complex three-dimensional (3D) micro/nanostructures, wherein a photosensitive liquid resin gets polymerized at the center of a tightly focused laser beam within a droplet, and the 3D digital model is built in a voxel-by-voxel manner [8].

A number of techniques have been investigated to create anisotropic composite nano/microstructures using the TPP process. For instance, Liu *et al.* investigated laser-directed self-alignment of silver nanoparticles within TPP resin [9]. Moreover, Masui *et al.* fabricated arbitrary micro-nano structured patterns using laser-assisted aggregation of Au nanorods [10]. However, in those works, the presented method can only align or orient the nanoparticles and has only been tested on letters and hollow structures, such as woodpile, with limited, precise control of local composition and patterning of nanoparticles within a polymer matrix.

An alternative strategy for particle patterning is the use of external force, such as magnetic [11,12], electric [13], or acoustic field [14–17]. However, applying these external fields at the nanoscale can result in very small force magnitudes and poor patterning accuracy and efficiency. Acoustophoresis is the most commonly used technique for generating anisotropic structures, especially in Stereolithography (SLA) and Direct Ink Writing (DIW) processes. However, in these studies, the particle size and patterning width are limited, and localized control of pattern is wavelength-dependent. Recently, the acoustic field (AF) has gained much attention for its potential in generating internal flows and patterning of NPs within a liquid droplet as small as 1 nL in volume [18]. It has been demonstrated through theoretical and numerical studies that below a frequency-dependent critical particle size (usually at a nanometer scale), the acoustic streaming induced drag forces keep the nanoparticles in constant motion driven by fluid flow [19].

* Corresponding author.
E-mail addresses: klicha2@uic.edu (K.M. Lichade), shanhu@iastate.edu (S. Hu), yayuepan@uic.edu (Y. Pan).

https://doi.org/10.1016/j.mfglet.2021.09.001

Based on this background, in this study, we demonstrate for the first time that acoustic field-assisted streaming can be used to fabricate anisotropic composite structures using the TPP process. Specifically, we show that the alignment of nanoparticles into the desired pattern at the microscale is possible using the acoustic streaming and trapping of nanoparticles within the grooved surface by controlling the input voltage and TPP manufacturing process. The input voltage was optimized to produce desired patterns with a width as small as 2 μm. From various surface structures, the inverse tapered groove shape was selected as it has been proven to be the most efficient design for high particle trapping efficiency [20]. By applying the AF, we established the relationship between the input voltage and flow velocity. Based on this relationship, we applied different flow velocity magnitudes to achieve the highest patterning efficiency of nanoparticles within a TPP fabricated groove space. After particle trapping, the nanoparticle-filled groove space was then polymerized by continuing the TPP process. This procedure is repeated in a layer-by-layer fashion until the last layer, to fabricate the desired 3D anisotropic composite model. We call this novel manufacturing process Acoustic Streaming-assisted Two-Photon Polymerization (AS-TPP). The AS-TPP fabricated microstructures were analyzed using optical, phase-contrast images and energy-dispersive spectrometer measurement (EDS), to validate the material distribution anisotropy and the manufacturing capability of the novel AS-TPP technology.

2. Materials and methods

2.1. Material and acoustic streaming-assisted two-photon polymerization (AS-TPP) setup

In this study, synthetic black iron oxide spherical magnetic nanoparticles (MNPs) (Alpha Chemical, USA) with an average diameter of 20 nm were used as functional fillers. IP-L 780 photoresist (Nanoscribe GmbH, Germany) was used as the base polymer material. The procedure for the material preparation is illustrated in Fig. 1a. First, MNPs were added to isopropyl alcohol (IPA), and the solution underwent ultrasonic agitation (2 min @ 60 W, U.S. Solid, USA) to clean and remove large MNP aggregates. Excess IPA was removed using centrifugation (60 min @ 4000 rpm) followed by complete evaporation by precipitation. The remnant MNPs (0.5 wt%) were dispersed in IP-L and 1 wt% Irgacure 369 (Sigma-Aldrich, USA) solution and the mixture was vigorously stirred for 24 h. The solution was then purified using centrifugation (30 min @4000 rpm) to remove large aggregates from the composite mixture; thus, the final composite would have a smaller 'effective' nanoparticle weight ratio. In our previous work, the polymerization threshold of IP-L and photothermal instability of 0.5 wt% MNPs were measured 6.6 mW (22%) and 5.7 mW (19%), respectively. Therefore, to eliminate the photothermal effect caused by high laser irradiation and enable successful polymerization, the polymerization threshold of IP-L resin was decreased from 6.6 mW to 5.7 mW by adding 10 wt% thiol molecules prior to printing [24].

Borosilicate glass with a thickness of 170 μm was cleaned with acetone for 1 min, and a rectangular-shaped piezoelectric plate (L: 20 mm, W: 15 mm, H: 1 mm) was attached on the top to generate acoustic waves (Steiner & Martins, Inc., Davenport, USA). A commercial Two-Photon Polymerization (TPP) (Nanoscribe GmbH, Germany) setup was retrofitted using the conventional oil immersion mode (63x objective) by integrating the acoustic setup into the commercial system, as shown in Fig. 1b. In the system, a femtosecond pulsed laser emitting at 780 nm, with a pulse width of 100 fs and a repetition rate of 80 MHz, was used as the light source to polymerize the anisotropic composites.

2.2. Fabrication of anisotropic composites

The CAD model and geometric parameters of the grooved surface design used in this study is shown in Fig. 2a, where W_t, W_b, and D are the top width, bottom width and depth of the groove. The total length of the surface is L. It has been demonstrated that the efficient nanoparticle trapping is dependent on the ratio of groove depth (D) and top width (W_t). Furthermore, these dimensions should be selected in such a way that the ratio of D/W_t is 0.5 and $W_b > W_t$, which was found to be the optimum design for efficient particle trapping [20–22]. The AS-TPP fabrication of an anisotropic composite layer consists of three steps: (1) curing the pure polymer region of the layer using TPP process while leaving the particle-filled region empty with an inverse tapered groove design, (2) AF-assisted microcirculation and trapping of MNPs in the grooved space of the layer, and (3) curing the MNPs-polymer composite in the grooved space using TPP.

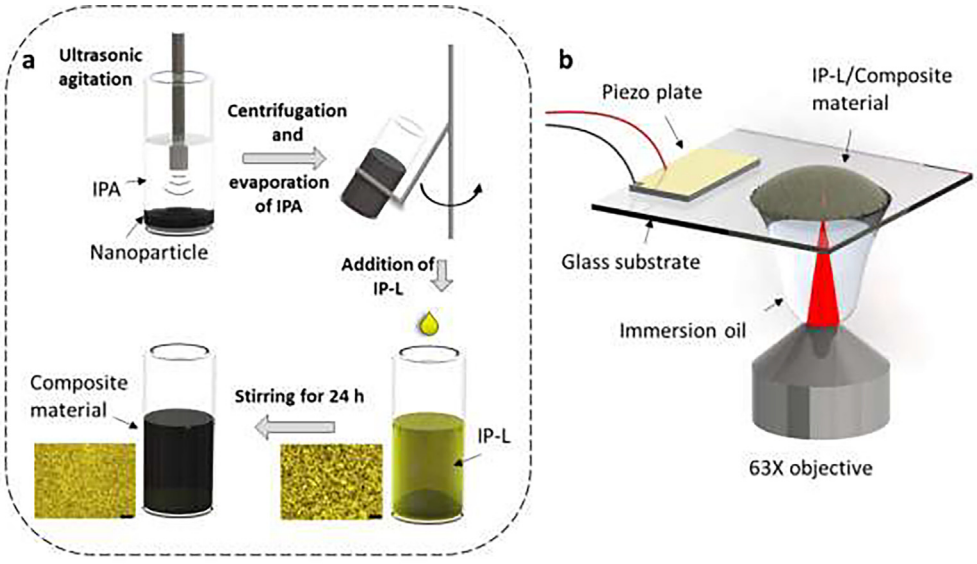

Fig. 1. Schematic of (a) material preparation procedure (Scale bar: 100 μm), (b) experimental setup for the AS-TPP process.

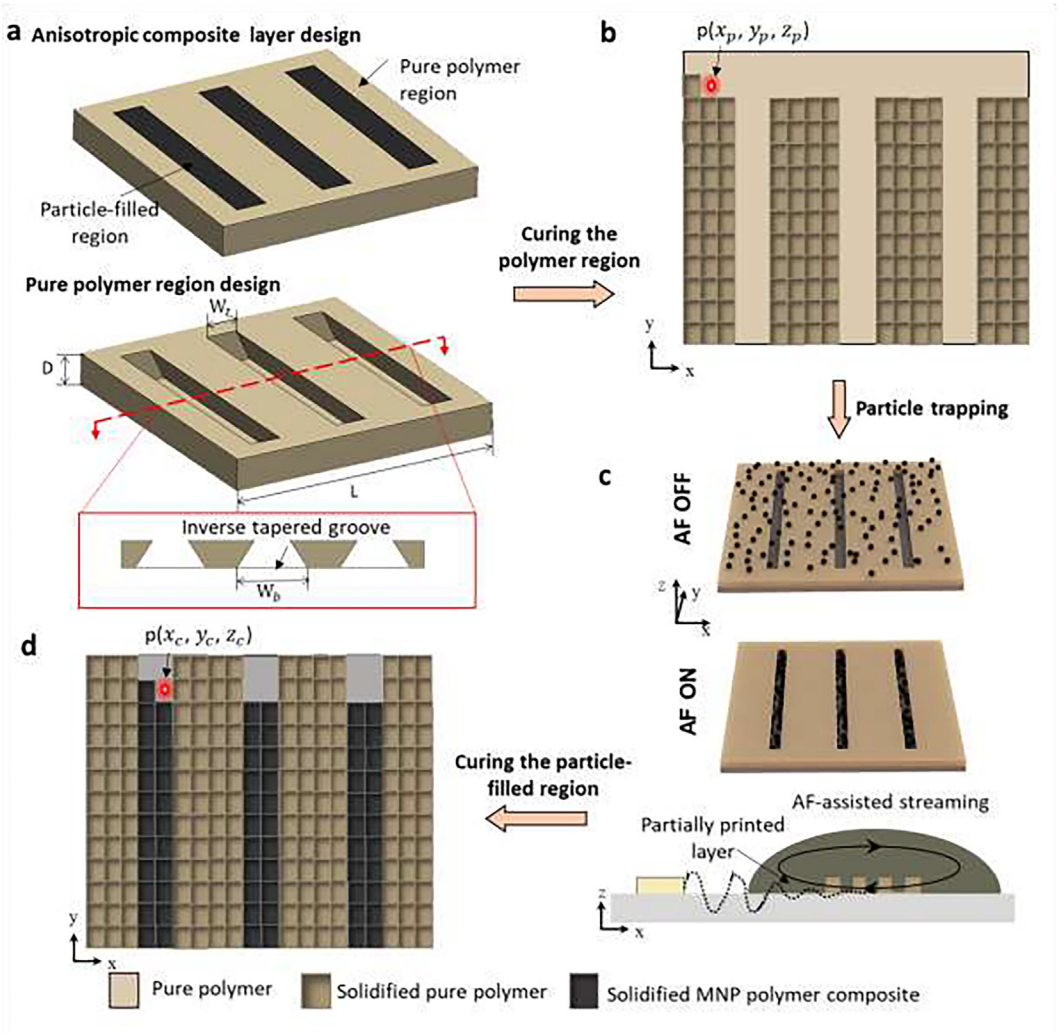

Fig. 2. Schematic of the AS-assisted Two-Photon Polymerization process (AS-TPP) for printing the anisotropic composite layer: (a) CAD model of the particle-filled anisotropic composite layer (top): the particle-filled region is designed with an inverse tapered shape with the $W_t < W_b$ (bottom); (b) two-photon polymerization of the pure polymer region of the layer at the desired voxels $p(x_p, y_p, z_p)$, (c) MNPs trapping within the inverse tapered grooves by AF-assisted particle streaming, (d) two-photon polymerization of particle-polymer composite within the groove spaces at the desired voxels $p(x_c, y_c, z_c)$.

To be more specific, a drop of IP-L photoresin (~3 mm) was placed on the coverslip, and the pure polymer region of the layer is photo-polymerized using TPP according to the voxel location, p (x_p, y_p, z_p), generated using GWL code (Describe software, Nanoscribe GmbH, Germany), and the particle-filled region is left uncured with an inverse tapered groove shape, as shown in Fig. 2b. The laser power and scanning speed was 6.6 mW (22%) and 10000 μm/s. The slicing and hatching distance was 0.2 μm and 0.2 μm, respectively. The glass coverslips containing these grooved surfaces were washed with SU-8 and IPA to remove the uncured resin.

Then a composite drop (~10 mm) was placed onto the grooved area of the printed layer, and AF was actuated at the resonance frequency of 1.1 MHz with varied input voltages. A high-frequency signal generator (RIGOL Technologies Inc., USA) and an amplifier (TEGAM Inc., USA) were used to generate sinusoidal signals. Upon actuation of AF, MNPs start streaming within the liquid droplet with varied velocity magnitude and direction, depending on the input voltage and their locations [23]. This AF-assisted streaming formed microcirculation within the grooves and resulted in nanoparticle trapping, as illustrated in Fig. 2c. Finally, after successfully trapping MNPs, the TPP process continued to cure the particle-polymer composite inside the grooves based on the voxel location, $p(x_c, y_c, z_c)$, generated using GWL code (Fig. 2d). To eliminate bubbling due to the photothermal effect and ensure successful printing, a laser power of 5.7 mW (19%) with a scanning speed of 10000 μm/s was selected [24]. This procedure is repeated until the last layer is printed. The uncured resin was washed away using SU-8 (MicroChem Corp., USA) for 9 min and IPA (Sigma-Aldrich, USA) for 2 min, followed by air drying and heat curing for 45 s.

3. Results and discussion

A schematic of the top view of particle streaming within a composite droplet before and after AF actuation is illustrated in Fig. 3a. When an AF field is applied, the flow direction is uniform at the center of the droplet but not in the boundary. Moreover, the local magnitude and direction of flow velocity depend on its position within the liquid droplet. As mentioned by Chen et al. [25] and Zhang et al. [26], the magnitude of flow velocity is directly proportional to the acoustic input voltage. The flow velocity is the critical parameter for the efficient trapping of particles within the groove space [22,27].

Here, we experimentally characterized the relationship between the input voltage and flow velocity. Four different ampli-

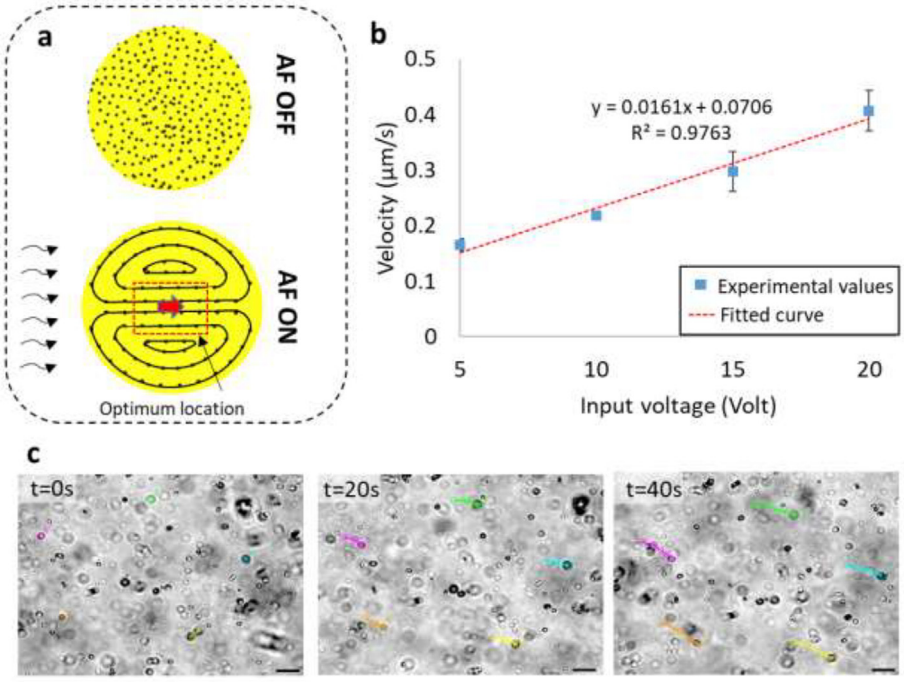

Fig. 3. (a) Illustration of streaming patterns and velocity direction induced by AF actuation, (b) relationship between acoustic input voltage and flow velocity, (c) the time-lapse images and particle trajectories at a velocity of 0.41 μm/s. Scale bar: 10 μm.

tudes of input voltage (V_{pp}) were tested using the developed setup, including 5, 10, 15, and 20 Volts. The movement of MNPs under these four different input voltages was recorded for 40 s using Axio Observer microscope and AxioVision software (ZEISS, USA). The velocity magnitude (S) of each particle was determined by analyzing the recorded images using ImageJ software. It is validated that the magnitude of flow velocity increases linearly with the input voltage, as shown in Fig. 3b. The square dots in the center of each error bar represent the average value of the measured velocity, while the solid line segment is the one standard deviation of the measured data. Five replicates were performed. Based on the observed values, the quantitative relationship between the input voltage and flow velocity can be fitted as the following equation:

$$S = 0.0161V_{pp} + 0.0706 \quad (1)$$

In addition, the time-lapse images and five particle trajectories using different colors at a velocity of 0.41 μm/s are shown in Fig. 3c. It can be seen that the MNPs moved in a uniform direction, indicating that the experiment was conducted at the center of the droplet.

To experimentally evaluate the dependency of the trapping efficiency on flow velocity, microgrooves with a dimension of W_t:

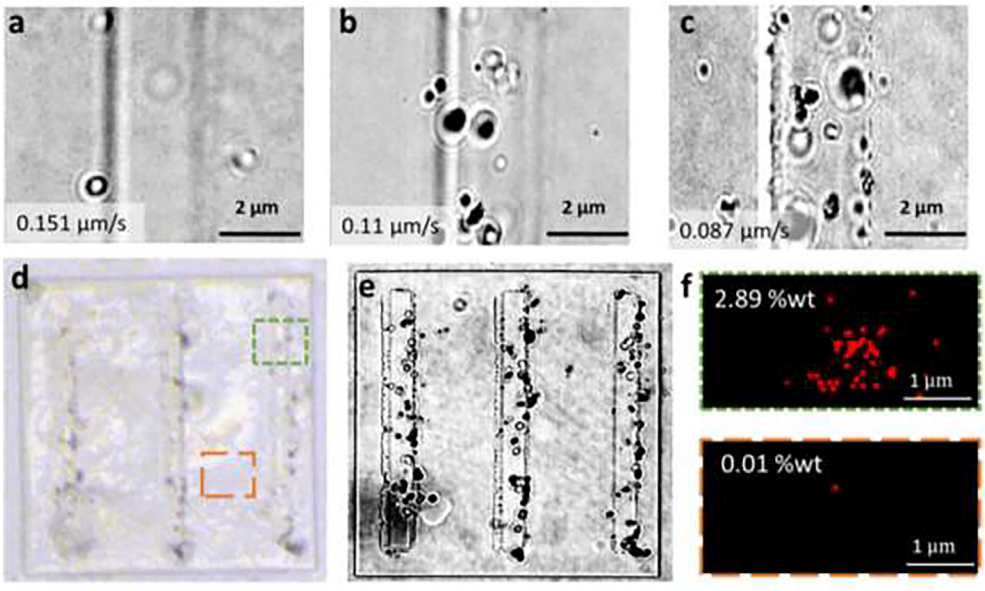

Fig. 4. Phase-contrast images of trapped nanoparticles within microgroove on the polymer layer surface with a flow velocity of (a) 0.151 (b) 0.11 and (c) 0.087, (d) optical image of nanoparticle-polymer composite structure, (e) phase-contrast image of nanoparticle-polymer composite structure (f) EDS distribution maps of element Fe in the two blocks in (d).

2 μm, W_b: 3 μm, and D: 1 μm were designed and fabricated on the glass substrate. Influence of flow velocities ranging from 0.151 to 0.41 μm/s on the particle trapping effectiveness was investigated. Eq. (1) was used to identify the voltage required for achieving different flow velocities. Experiment results revealed that the nanoparticle trapping was significantly weakened to a negligible state with the flow velocity increased from 0.151 to 0.41 μm/s. The smaller flow velocity from 0.151 to 0.087 μm/s resulted in increased nanoparticle trapping. Figs. 4a–c show the phase-contrast images of MNPs trapped within grooves at smaller flow velocities. Using Eq. (1), the corresponding input voltage for achieving velocities of 0.151, 0.11, and 0.087 μm/s was calculated as 5, 2.5, and 1 V, respectively. It can be seen that the concentration of trapped MNPs is the highest at the flow velocity of 0.087 μm/s.

After finding the optimum velocity for efficient trapping, a 30 (L) by 30 (L) μm anisotropic composite structure with three parallel particle lines (W_t: 2 μm, W_b: 3 μm, and D: 1 μm) was fabricated using the proposed 3-step fabrication process. The optical and phase-contrast images of the fabricated anisotropic composites are shown in Figs. 4d and e, respectively. We also quantified the distribution and weight percentage of MNPs using EDS (JSM-IT500HR FESEM, JEOL, Europe) measurement, as shown in Fig. 4f. It can be determined that the red area is the distribution map of the Fe element, and the black area is the pure polymer. The Fe content within the micro-groove was around 2.89%. In contrast, a negligible nanoparticle concentration (0.01%) was observed in other regions. The experimental results verified that the proposed AS-TPP process could be used to fabricate anisotropic composites with desired nanoparticle assemblies. Moreover, it can be expected that by tuning experimental parameters, such as input voltage, feedstock nanoparticle concentration, and groove dimensions, it is possible to achieve a higher particle concentration and complex assembly patterns.

4. Conclusion

A novel method for fabricating anisotropic composite structures based on Acoustic Streaming-assisted Two-Photon Polymerization (AS-TPP) is presented in this study. Instead of wavelength-dependent patterning, we used AF-assisted streaming to trap nanoparticles inside the TPP printed grooved polymer surface and further solidifying the groove space consisting of trapped MNPs. Applying the proposed method allows precise control of nanoparticle patterns and localized distribution within a polymer matrix. Furthermore, the flow velocity can be adjusted by controlling the acoustic input voltage to achieve the desired trapping efficiency. The results shown in this work are promising and can be further developed to fabricate functional composite microstructures for various applications. For instance, by integrating hydrophilic nanoparticles in the anisotropic composite structures during the AS-TPP process, well-defined wettability patterns can be generated. These high-resolution patterned surfaces with wettability contrast enable properties such as excellent liquid manipulation and directional droplet transport, making them ideal for potential applications, including microfluidic devices, cell movement control, lab-on-chip devices, and controlled drug release coatings.

Future work will focus on optimizing the polymer surface groove geometry using Finite Element Analysis (FEA) methods to improve the particle trapping efficiency and weight ratio and test more complicated particle patterns.

Declaration of Competing Interest

The authors declare that they have no known competing financial interests or personal relationships that could have appeared to influence the work reported in this paper.

Acknowledgement

This material is based upon work partially supported by the United States National Science Foundation under Grant Number # 1663399.

References

[1] Ushiba S, Shoji S, Masui K, Kuray P, Kono J, Kawata S. 3D microfabrication of single-wall carbon nanotube/polymer composites by two-photon polymerization lithography. Carbon N Y 2013;59:283–8. https://doi.org/10.1016/j.carbon.2013.03.020.
[2] Roy M, Tran P, Dickens T, Schrand A. Composite Reinforcement Architectures: A Review of Field-Assisted Additive Manufacturing for Polymers. J Compos Sci 2019;4:1. https://doi.org/10.3390/jcs4010001.
[3] Joyee EB, Lu Lu, Pan Y. Analysis of mechanical behavior of 3D printed heterogeneous particle-polymer composites. Compos Part B Eng 2019;173:106840. https://doi.org/10.1016/j.compositesb.2019.05.051.
[4] Kabashin AV, Evans P, Pastkovsky S, Hendren W, Wurtz GA, Atkinson R, et al. Plasmonic nanorod metamaterials for biosensing. Nat Mater 2009;8(11):867–71. https://doi.org/10.1038/nmat2546.
[5] Skylar-Scott MA, Gunasekaran S, Lewis JA. Laser-assisted direct ink writing of planar and 3D metal architectures. Proc Natl Acad Sci U S A 2016;113(22):6137–42. https://doi.org/10.1073/pnas.1525131113.
[6] Qiao Z, Yang X, Yang S, Zhang L, Cao B. 3D hierarchical MnO2 nanorod/welded Ag-nanowire-network composites for high-performance supercapacitor electrodes. Chem Commun 2016;52(51):7998–8001. https://doi.org/10.1039/C6CC03768B.
[7] Kaneko A, Takeda I. Textured surface of self-assembled particles as a scaffold for selective cell adhesion and growth. Int J Autom Technol 2016;10:62–8. https://doi.org/10.20965/ijat.2016.p0062.
[8] Lichade K, Jiang Y, Pan Y. Hierarchical nano/micro-structured surfaces with high surface area/volume ratios. J Manuf Sci Eng 2021:1–36. https://doi.org/10.1115/1.4049850.
[9] Liu Y, Xiong W, Li DW, Lu Y, Huang Xi, Liu H, et al. Precise assembly and joining of silver nanowires in three dimensions for highly conductive composite structures. Int J Extrem Manuf 2019;1(2):025001. https://doi.org/10.1088/2631-7990/ab17f7.
[10] Masui K, Shoji S, Asaba K, Rodgers TC, Jin F, Duan X-M, et al. Laser fabrication of Au nanorod aggregates microstructures assisted by two-photon polymerization. Opt Express 2011;19(23):22786. https://doi.org/10.1364/OE.19.022786.
[11] Lu, Guo P, Pan Y. Magnetic-Field-Assisted Projection Stereolithography for Three-Dimensional Printing of Smart Structures. J Manuf Sci Eng Trans ASME 2017;139. https://doi.org/10.1115/1.4035964.
[12] Martin JJ, Fiore BE, Erb RM. Designing bioinspired composite reinforcement architectures via 3D magnetic printing. Nat Commun 2015;6:1–7. https://doi.org/10.1038/ncomms9641.
[13] Yang Y, Chen Z, Song X, Zhang Z, Zhang J, Shung KK, et al. Biomimetic Anisotropic Reinforcement Architectures by Electrically Assisted Nanocomposite 3D Printing. Adv Mater 2017;29. https://doi.org/10.1002/adma.201605750.
[14] Yunus DE, Sohrabi S, He R, Shi W, Liu Y. Acoustic patterning for 3D embedded electrically conductive wire in stereolithography. J Micromech Microeng 2017;27(4):045016. https://doi.org/10.1088/1361-6439/aa62b7.
[15] Collino RR, Ray TR, Fleming RC, Cornell JD, Compton BG, Begley MR. Deposition of ordered two-phase materials using microfluidic print nozzles with acoustic focusing. Extrem Mech Lett 2016;8:96–106. https://doi.org/10.1016/j.eml.2016.04.003.
[16] Hahnlen R, Dapino MJ. NiTi-Al interface strength in ultrasonic additive manufacturing composites. Compos Part B Eng 2014;59:101–8. https://doi.org/10.1016/j.compositesb.2013.10.024.
[17] Lu Lu, Tang X, Hu S, Pan Y. Acoustic field-assisted particle patterning for smart polymer composite fabrication in stereolithography. 3D Print Addit Manuf 2018;5(2):151–9. https://doi.org/10.1089/3dp.2017.0157.
[18] Shilton RJ, Travagliati M, Beltram F, Cecchini M. Nanoliter-droplet acoustic streaming via ultra high frequency surface acoustic waves. Adv Mater 2014;26(29):4941–6. https://doi.org/10.1002/adma.v26.2910.1002/adma.201400091.
[19] Fakhfouri A, Devendran C, Ahmed A, Soria J, Neild A. The size dependant behaviour of particles driven by a travelling surface acoustic wave (TSAW). Lab Chip 2018;18(24):3926–38. https://doi.org/10.1039/C8LC01155A.
[20] Florio LA. Numerical investigation of particle trapping in various groove configurations in straight and bent flow channels. Simulation 2020;96(8):679–99. https://doi.org/10.1177/0037549720922600.
[21] Cioffi M, Moretti M, Manbachi A, Chung BG, Khademhosseini A, Dubini G. A computational and experimental study inside microfluidic systems: the role of shear stress and flow recirculation in cell docking. Biomed Microdevices 2010;12(4):619–26. https://doi.org/10.1007/s10544-010-9414-5.
[22] Manbachi A, Shrivastava S, Cioffi M, Chung BG, Moretti M, Demirci U, et al. Microcirculation within grooved substrates regulates cell positioning and cell docking inside microfluidic channels. Lab Chip 2008;8(5):747. https://doi.org/10.1039/b718212k.
[23] Norsuzila Ya'acob1, Mardina Abdullah1, 2 and Mahamod Ismail1 2, Medina M, Talarico TL, Casas IA, Chung TC, Dobrogosz WJ, et al. We are IntechOpen, the

world' s leading publisher of Open Access books Built by scientists, for scientists TOP 1 %. Intech 1989;32:137–44.
[24] Lichade KM, Pan Y. Acoustic field-assisted two-photon polymerization process. J Manuf Sci Eng 2021;143:1–7. https://doi.org/10.1115/1.4050759.
[25] Chen M, Cai F, Wang C, Wang Z, Meng L, Li F, et al. Observation of metal nanoparticles for acoustic manipulation. Adv Sci 2017;4(5):1600447. https://doi.org/10.1002/advs.v4.510.1002/advs.201600447.
[26] Zhang C, Guo X, Brunet P, Costalonga M, Royon L. Acoustic streaming near a sharp structure and its mixing performance characterization. Microfluid Nanofluidics 2019;23(9). https://doi.org/10.1007/s10404-019-2271-5.
[27] Ramazani Sarbandi I, Taslimi MS, Bazargan V. Novel criteria for the optimum design of grooved microchannels based on cell shear protection and docking regulation: a lattice Boltzmann method study. SN Appl Sci 2020;2:1–14. https://doi.org/10.1007/s42452-020-03630-0.